Numerical Assessment of the Stiffness Index*

Sally Epstein[1], Anne-Claire Vergnaud[2], Paul Elliott[3], Phil Chowienczyk[3] and Jordi Alastruey[1]

***Abstract*— Elevated systemic vascular stiffness is associated with increased risk of cardiovascular disease. It has been suggested that the time difference between the two characteristic peaks of the digital volume pulse (DVP) measured at the finger using photoplethysmography is related to the stiffness of the arterial tree, and inversely proportional to the stiffness index (SI). However, the precise physical meaning of the SI and its relation to aortic pulse wave velocity (aPWV) is yet to be ascertained. In this study we investigated numerically the effect of changes in arterial wall stiffness, peripheral resistances, peripheral compliances or peripheral wave reflections on the SI and aPWV. The SI was calculated from the digital area waveform simulated using a nonlinear one-dimensional model of pulse wave propagation in a 75-artery network, which includes the larger arteries of the hand. Our results show that aPWV is affected by changes in aortic stiffness, but the SI is primarily affected by changes in the stiffness of all conduit vessels. Thus, the SI is not a direct substitute for aPWV. Moreover, our results suggest that peripheral reflections in the upper body delay the time of arrival of the first peak in the DVP. The second peak is predominantly caused by the impedance mismatch within the 75 arterial segments, rather than by peripheral reflections.**

I. INTRODUCTION

Stiffening of large elastic arteries such as the aorta is a hallmark of vascular ageing [1], and as measured by aortic pulse wave velocity (aPWV) is highly predictive of clinical manifestations of cardiovascular disease [2], which is the biggest single cause of mortality in the developed world [3]. Variations in arterial stiffness produce profound changes in the contour of the arterial pulse wave [4], demonstrating the potential of pulse wave analysis to provide a measure of arterial stiffness.

Photoplethysmography is a simple non-invasive technique to register the digital volume pulse (DVP) at the finger, which is closely related to the peripheral pressure pulse [5]. It has been suggested that aPWV can be estimated from the DVP through the calculation of a stiffness index (SI) defined as [6]

$$\mathrm{SI} = \frac{H}{\mathrm{PPT}}, \tag{1}$$

where H is the subject height and PPT denotes the peak-to-peak time of the DVP contour (Fig. 1b).

The SI has been used to assess arterial ageing [6], is sensitive in detecting premature arterial stiffening in young adults [7], and has been recorded in over 185,000 participants of the on-going UK Biobank project [8]. Thus, understanding the physical meaning of the SI and its relation to aPWV is very important to advance cardiovascular epidemiology, but this has not been achieved yet. It has been hypothesised that the distinct two-peaked undulatory form of the DVP is due to pressure waves travelling from the left ventricle to the finger and later smaller reflections from internal mismatching mainly in the lower body [4]. The path length that reflected waves travel is assumed to be proportional to H.

The aim of this study is to investigate numerically (i) how changes in arterial wall stiffness, peripheral resistances or peripheral compliances affect the SI and aPWV and (ii) the effect of peripheral wave reflections on the arrival time of the two characteristic peaks of the DVP contour.

II. METHODS

We simulated the DVP contour by solving the nonlinear one-dimensional (1-D) equations of blood flow in compliant vessels in the 75-artery network shown in Fig. 1a. These equations can be derived from the physical principles of conservation of mass and momentum, assuming the arterial wall to be a thin, homogenous, incompressible and elastic material [9], [10]. Several comparisons against *in vivo* [11], *in vitro* [12] and three-dimensional numerical [13] data have shown the ability of the 1-D formulation to capture the main features of pressure and flow waveforms in human arteries.

The properties of Segments 1 to 55 were taken from [14] based on data for an average young adult with a height $H = 178 \pm 12$ cm [11]. Segments 56 to 75 correspond to the arterial segments of the hands (digital arteries and superficial and deep palmar arches) and have the properties described in [15]. At the proximal end of the aorta (Segment 1) we prescribed the flow waveform shown in Fig. 1a, which was acquired using phase-contrast magnetic resonance imaging in a healthy young adult with $H = 175$ cm. The distal end of each terminal vessel was coupled to a three-element Windkessel model of the perfusion of the microcirculation, consisting of two peripheral resistances (R_1 and R_2) and one compliance (C). Further details on the 1-D formulation and its numerical solution are given in [12].

The SI was calculated using the PPT obtained from the luminal area waveform in the midpoint of the middle digital artery of the right hand (Segment 60), under the assumption that digital area changes are proportional to the blood volume

*This work was supported by the Centre of Excellence in Medical Engineering (funded by the Wellcome Trust and EPSRC under grant number WT 088641/Z/09/Z) and the National Institute for Health Research (NIHR) Biomedical Research Centre at Guy's and St Thomas' NHS Foundation Trust in partnership with King's College London. J. A. also acknowledges support from the British Heart Foundation (FS/09/030/27812).

[1]S. Epstein and J. Alastruey are with the Department of Biomedical Engineering, St Thomas' Hospital, King's College, London SE1 7EH, United Kingdom.

[2]A.-C. Vergnaud and P. Elliott are with the Department of Epidemiology and Biostatistics, St Mary's Hospital, Imperial College, London W2 1PG, United Kingdom.

[3]P. Chowienczyk is with the Department of Clinical Pharmacology, St Thomas' Hospital, King's College, London SE1 7EH, United Kingdom.

978-1-4244-7929-0/14/$26.00 ©2014 IEEE

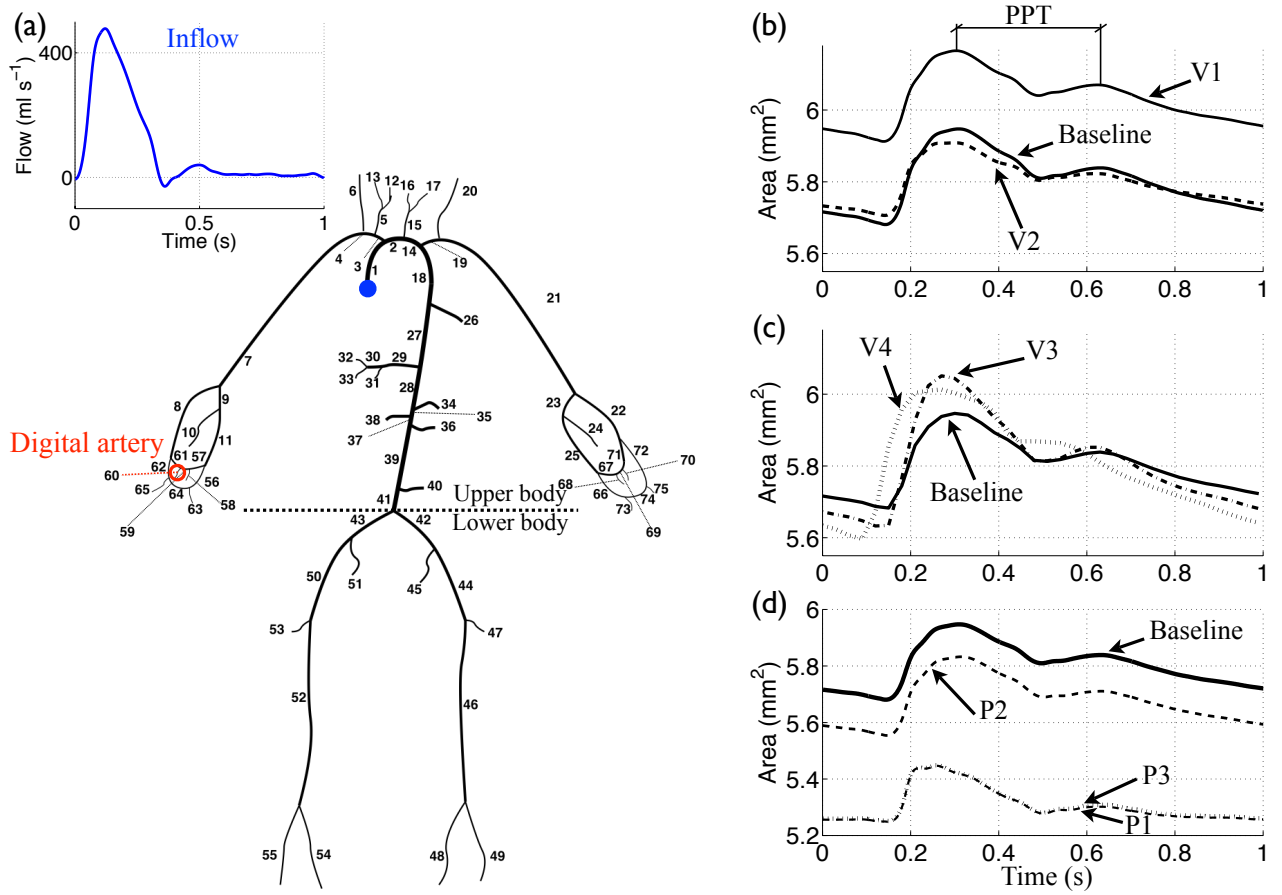

Fig. 1. (a) Schematic representation of the 75-artery model showing the flow waveform prescribed at the inlet of the ascending aorta (Segment 1) as a reflective boundary condition. (b) Simulated luminal area waveform in the midpoint of the middle digital artery of the right hand (Segment 60) in normal conditions (baseline model) and with a 50% increase in peripheral resistances (V1) or a 200% increase in peripheral compliances (V2) from the corresponding baseline values. (c) Area waveform in Segment 60 at baseline and with a 200% increase in aortic stiffness (V3) or a 200% increase in conduit stiffness (V4) from the corresponding baseline values. The theoretical aPWV was calculated in the midpoint of Segment 1 and the stiffness index was computed from the peak-to-peak time (PPT) of the area contour in Segment 60. (d) Area waveform in Segment 60 at baseline and under the three different combinations of absorbing and Windkessel outflow boundary conditions described in Table I.

TABLE I
TYPES OF PERIPHERAL BOUNDARY CONDITIONS STUDIED

Model	Upper Body	Lower Body
Baseline	Windkessel	Windkessel
P1	Absorbing	Absorbing
P2	Windkessel	Absorbing
P3	Absorbing	Windkessel

Boundary conditions are either baseline Windkessel or completely absorbing. The model is divided into upper- and lower-body arterial segments, as illustrated in Fig. 1a.

changes measured by the DVP contour. The theoretical aPWV was calculated in the midpoint of the ascending aorta (Segment 1) using the parameters of the model at mean blood pressure.

A. Changes in Baseline Properties

We investigated the effects on the SI of changes in peripheral resistances, peripheral compliances or the stiffness of the arterial wall of the 75-artery model (Fig. 1a) described above (hereinafter referred to as *baseline model*). We considered the following four types of variations from the baseline model:

- *Variation V1 – Changes in peripheral resistance*: The resistance $R_1 + R_2$ was modified in all terminal Windkessel models by the same percentage to simulate changes in net peripheral resistance from $0.65 \cdot 10^8$ to $3.28 \cdot 10^8$ Pa s m^{-3}, based on the values reported in [16]. 12 variations from the baseline model were considered. The baseline resistance is $1.09 \cdot 10^8$ Pa s m^{-3}.
- *Variation V2 – Changes in peripheral compliance*: The compliance C was modified in all terminal Windkessel models by the same percentage to simulate changes in total systemic compliance from $1.05 \cdot 10^{-8}$ to $1.92 \cdot 10^{-8}$ m^3 Pa^{-1}, based on the values reported in [17]. 13 variations from the baseline model were considered taking into account that the total systemic compliance is the sum of the total compliance of the 75 arterial segments and the total peripheral compliance [18]. At baseline, the total peripheral compliance is $0.45 \cdot 10^{-8}$ m^3 Pa^{-1} and the total systemic compliance is $1.25 \cdot 10^{-8}$ m^3 Pa^{-1}.
- *Variation V3 – Changes in aortic stiffness*: The elastic

moduli of all the aortic segments (1, 2, 14, 18, 27, 28, 35, 37, 39 and 41) were changed by -25% to 300% of the baseline values. A total of 16 variations from baseline values were considered. As a result, the baseline aPWV= 4.0 m s^{-1} changed from 3.6 to 7.9 m s^{-1}, which is a physiologically possible range of values [19]. Note that in our model pulse wave velocity (PWV) is proportional to the square of elastic modulus [18].

- *Variation V4 – Changes in conduit stiffness*: The changes in elastic moduli of V3 were extended to all but the terminal arterial segments.

B. Changes in Peripheral Wave Reflections

We investigated the contribution to the baseline area waveform at the finger (Segment 60) of wave reflections originating at the outlet of terminal branches, which we referred to as *peripheral reflections*. As described in [18], peripheral reflections can be eliminated from a terminal branch if the outflow three-element Windkessel model is replaced by a single resistance equal to the characteristic impedance at the outlet of the branch, so that any wave leaving the terminal branch is completely absorbed by the outlet. We considered the combination of baseline Windkessel and completely absorbing boundary conditions described in Table I. For this study we divided the 75 arterial segments in Fig. 1a into two subsets: *upper-body* segments located above the iliac bifurcation and *lower-body* segments located below the iliac bifurcation.

III. RESULTS & DISCUSSION

The simulated digital area waveform at baseline (Fig. 1b) contains the two peaks that characterise the DVP measured *in vivo* [5], [6], leading to a SI $= 5.4$ m s^{-1}. Alterations in peripheral resistances or compliances, aortic stiffness, arterial stiffness, or peripheral reflections produce considerable variations in the shape of the area contour, but not all these alterations change considerably the PPT, and, hence, SI. We discuss these results below.

A. Effect of Resistance, Compliance and Wall Stiffness on SI

Alterations in conduit stiffness cause the greatest changes in SI within the physiological range of variations in the model properties shown in Fig. 2: a 200% increase in the elastic moduli of all but terminal vessels increases SI by over 60%, whereas a 200% increase in peripheral resistances or compliances yields changes in SI smaller than 2%. This is because peripheral resistances affect mainly the magnitude of the digital area waveform, whereas peripheral compliances affect mainly the amplitude of the waveform (Fig. 1b). These variations in area waveforms are in agreement with the well-known increase in mean blood pressure with increasing peripheral resistance and decrease in pulse pressure with increasing peripheral compliance [20], which are all well captured by our model (results not shown). Area and pressure changes follow a similar pattern because they are directly related through Laplace's law [20], [12].

Neither peripheral resistances nor peripheral compliances produce considerable changes in the PPT (and hence SI), which suggests that the PPT results from wave propagation and reflection phenomena within the 1-D domain and is not primarily affected by peripheral wave reflections. Variations in wall stiffness yield greater changes in PPT because they produce larger variations in PWV than changes in peripheral resistances or compliances, as shown in Fig. 2 for the aPWV. aPWV raises with increasing peripheral resistances (Fig. 2a) because aPWV increases with blood pressure.

The predicted raise in PWV with increasing arterial stiffness is physiological [20] and changes the time of arrival of the foot and peaks of the digital area waveform (Fig. 1c). These arrive earlier with increased conduit stiffness than increased aortic stiffness, since the latter only decreases the transit along the aorta. For example, compared to baseline, the foot arrives 60 ms earlier with a conduit stiffness 200% greater than baseline values, but only 5 ms earlier with the same percentage increase in aortic stiffness. Moreover, alterations in conduit stiffness cause greater changes in the PPT (and hence SI) than alterations in aortic stiffness (Fig. 2c,d). The PPT decreases and the SI increases with increasing conduit stiffness (Fig. 2d), suggesting that the second peak is produced by reflections of wavefronts that make up the first peak, which arrive earlier at the digital artery with increased PWV (and hence decreased transit time) in all conduit arteries. However, if PWV is only increased in the aorta then our model predicts a raise in PPT leading to a slight drop in SI (Fig. 2c).

Increases in wall stiffness also raise the amplitude of the digital area waveform (Fig. 1c) due to the increase in pulse pressure caused by the Windkessel effect, as described in [14] using the 1-D formulation. The Windkessel effect is also responsible for the smaller changes in the amplitude of the digital area waveform introduced by alterations in peripheral compliance (Fig. 1b, V2).

B. Effect of Peripheral Reflections on SI

Fig. 1d (P1) shows that two peaks are still present in the digital area waveform without a change in their arrival time when all peripheral reflections have been removed from the baseline model. This result suggests that both peaks are predominantly made up of wavefronts propagating from the aortic root and their reflections at arterial junctions, tapered vessels, and the aortic root. However, peripheral reflections do affect the arrival time of the first peak: this arrives 52 ms earlier when peripheral reflections are absent.

Removing peripheral reflections from only the lower-body segments (P2) results in an area waveform with a greater magnitude than if peripheral reflections are removed from only upper-body segments (P3). This result indicates that peripheral reflections originating in the upper body have a greater contribution to the magnitude of the area waveform than do peripheral reflections originating in the lower body. The second peak arrives at approximately the same time in models P2 and P3, but the first peak arrives 52 ms earlier in model P3, suggesting that peripheral reflections in the

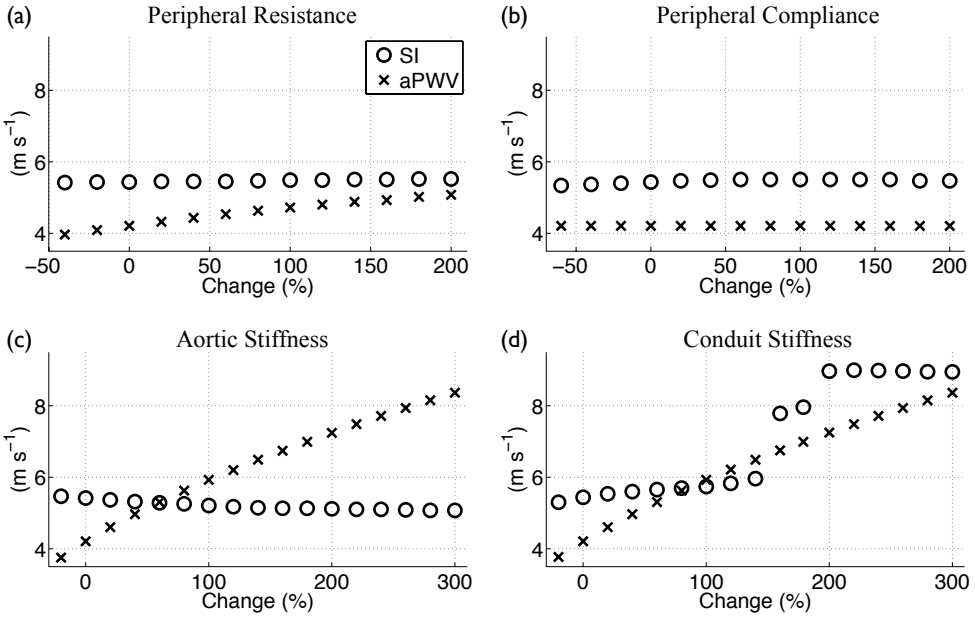

Fig. 2. Calculated aortic pulse wave velocity (aPWV, crosses) and stiffness index (SI, circles) with percentage changes from baseline in (a) net peripheral resistance, (b) total peripheral compliance, (c) aortic stiffness and (d) conduit stiffness, as described in Section II-A.

upper body delay the arrival time of the first peak and, hence, increase the SI by decreasing the PPT.

IV. CONCLUSIONS

Our numerical investigations have shown that the stiffness index is primarily affected by changes in conduit stiffness. Variations in peripheral compliances, peripheral resistances, or aortic stiffness, within physiological ranges, have a small influence on the stiffness index. Thus, the stiffness index is not a direct marker for aortic pulse wave velocity determined by changes in aortic stiffness.

REFERENCES

[1] A. P. Avolio, S. G. Chen, R. P. Wang, C. L. Zhang, M. F. Li, and M. F. O'Rourke, Effects of aging on changing arterial compliance and left ventricular load in a northern Chinese urban community, *Circulation*, vol. 68, no. 1, pp. 50–8, July 1983.

[2] C. Vlachopoulos, K. Aznaouridis, and C. Stefanadis, Prediction of cardiovascular events and all-cause mortality with arterial stiffness: A systematic review and meta-analysis, *J. Am. Coll. Cardiol.*, vol. 55, no. 13, pp. 1318–27, May 2010.

[3] C. Mathers, G. Stevens and M. Mascarenhas, *Global health risks: mortality and burden of disease attributable to selected major risks*. World Health Organization, 2009.

[4] P. J. Chowienczyk, R. P. Kelly, H. Maccallum, S. C. Millasseau, T. L. G. Andersson, R. G. Gosling, J. M. Ritter, and E. E. Anggård, Photoplethysmographic assessment of pulse wave reflection: Blunted response to endothelium-dependent beta$_2$-adrenergic vasodilation in type II diabetes mellitus, *J. Am. Coll. Cardiol.*, vol. 34, no. 7, pp. 2007–14, Dec. 1999.

[5] S. C. Millasseau, J. M. Ritter, K. Takazawa, and P. J. Chowienczyk, Contour analysis of the photoplethysmographic pulse measured at the finger, *J. Hypertens.*, vol. 24, no. 8, pp. 1449–56, Aug. 2006.

[6] S. C. Millasseau, R. P. Kelly, J. M. Ritter, and P. J. Chowienczyk, Determination of age-related increases in large artery stiffness by digital pulse contour analysis, *Clin. Sci. (Lond)*, vol. 103, no. 4, pp. 371–7, Oct. 2002.

[7] C. Broyd, E. Harrison, M. Raja, S. C. Millasseau, L. Poston, and P. J. Chowienczyk, Association of pulse waveform characteristics with birth weight in young adults, *J. Hypertens.*, vol. 23, no. 7, pp. 1391–6, June 2005.

[8] http://biobank.ctsu.ox.ac.uk/crystal/field.cgi?id=21021 (accessed June 2014)

[9] T. J. R. Hughes and J. Lubliner, On the one-dimensional theory of blood flow in the larger vessels, *Math. Biosc.*, vol. 18, pp. 161–70, 1973.

[10] S. J. Sherwin, V. Franke, J. Peiró, and K. Parker, One-dimensional modelling of a vascular network in space-time variables, *J. Eng. Math.*, vol. 47, no. 3-4, pp. 217–50, Dec. 2003.

[11] P. Reymond, F. Merenda, F. Perren, D. Rüfenacht, and N. Stergiopulos, Validation of a one-dimensional model of the systemic arterial tree, *Am. J. Physiol. Heart Circ. Physiol.*, vol. 297, pp. H208–22, May 2009.

[12] J. Alastruey, A. W. Khir, K. S. Matthys, P. Segers, S. J. Sherwin, P. R. Verdonck, K. H. Parker, and J. Peiró, Pulse wave propagation in a model human arterial network: Assessment of 1-D visco-elastic simulations against *in vitro* measurements, *J. Biomech.*, vol. 44, no. 12, pp. 2250–8, Aug. 2011.

[13] N. Xiao, J. Alastruey, and C. A. Figueroa, A systematic comparison between 1-D and 3-D hemodynamics in compliant arterial models, *Int. J. Numer. Meth. Biomed. Eng.*, vol. 30, no. 2, pp. 204–31, Feb. 2014.

[14] J. Alastruey, A. A. E. Hunt, and P. D. Weinberg, Novel wave intensity analysis of arterial pulse wave propagation accounting for peripheral reflections, *Int. J. Numer. Meth. Biomed. Eng.*, vol. 30, no. 2, pp. 249–79, Feb. 2014.

[15] J. Alastruey, K. H. Parker, J. Peiró, and S. J. Sherwin, Can the modified Allen's test always detect sufficient collateral flow in the hand? A computational study, *Comp. Meth. Biomech. Biomed. Eng.*, vol. 9, no. 6, pp. 353–61, Dec. 2006.

[16] J. R. C. Jansen, J. J. Schreuder, J. P. Mulier, N. T. Smith, J. J. Settels, and K. H. Wesseling, A comparison of cardiac output derived from the arterial pressure wave against thermodilution in cardiac surgery patients, *Br. J. Anaesth.*, vol. 87, no. 2, pp. 212–22, 2001.

[17] D. Chemla, J.-L. Hébert, C. Coirault, K. Zamani, I. Suard, P. Colin, and Y. Lecarpentier, Total arterial compliance estimated by stroke volume-to-aortic pulse pressure ratio in humans, *Am. J. Phys. Heart Circ. Phys.*, vol. 274, pp. H500–5, Feb. 1998.

[18] J. Alastruey, K. H. Parker, J. Peiró, and S. J. Sherwin, Analysing the pattern of pulse waves in arterial networks: a time-domain study, *J. Eng. Math.*, vol. 64, no. 4, pp. 331–51, Feb. 2009.

[19] M. F. O'Rourke, J. A. Staessen, C. Vlachopoulos, D. Duprez, and G. E. Plante, Clinical applications of arterial stiffness; definitions and reference values, *Am. J. Hypertens.*, vol. 15, no. 5, pp. 426–44, May 2002.

[20] D. A. McDonald, *Blood Flow in Arteries*. Williams & Wilkins, 1974.